blocks [26]. This method successfully improved the surface wettability and lubrication and decreased the biofouling tendency of PDMS. Although the modification of the PDMS surface with MPC via a chemical reaction is a powerful tool for enhancing the properties of PDMS, the process is complex and it is difficult to modify intricately shaped devices after fabrication. More practical methods have been reported by Sibarani et al., who modified the PDMS surface by a simple treatment method [27], and Seo et al., who modified the PDMS surface by swelling–deswelling methods using ABA-type block copolymers composed of PMPC (A) and PDMS (B) segments [28]. The relative simplicity of these processes renders them more applicable than grafting polymerization and chemical reaction processes. However, the disadvantage of these methods is that low-polarity solvents such as chloroform are used for the surface treatment process because of the low surface energy of PDMS. These solvents induce swelling of PDMS, and consequently, this method is unsuitable for tailor-made devices with dimension-specific designs. On the other hand, the adsorption of poly(ethylene oxide)-*block*-poly(propylene oxide)-*block*-poly(ethylene oxide) and poly(L-lysine)-*graft*-poly(ethylene glycol) (PLL-*g*-PEG) on hydrophobic surfaces in aqueous environments has been reported [29–31]. Lee et al. investigated the adsorption behavior of PLL-*g*-PEG on the PDMS surface by changing the molecular weight of the copolymer and varying the solvent parameters such as pH and salt concentration. They suggested that the large number of hydrophobic groups in the copolymer and the extended conformation of the polymer in aqueous solution are associated with the ease of adsorption of the polymer [31]. For surface modification of biomedical devices, stability of the adsorbed polymer layer under aqueous conditions is essential. In general, proteins can be readily adsorbed from an aqueous medium onto various surfaces. Surface adsorption is normally irreversible owing to conformational changes of the proteins on the surface. Although surface adsorption of protein is a complex process, hydrophobic interaction and electrostatic forces generated at the interface are some of the dominant forces [32]. When proteins approach a surface, the water molecules between surrounding proteins and the surface are removed by an entropic effect. This phenomenon induces a conformational change in the proteins, and the proteins are irreversibly adsorbed on the surface by hydrophobic interaction and electrostatic interaction. We hypothesized that a molecular design similar to the protein structure, with hydrophobic portions and electric charges, should be suitable for the surface treatment of PDMS. PDMS is an elastic material, its surface is hydrophobic, and its surface ζ potential is −44.1 mV [27]. Therefore, we chose 2-ethylhexyl methacrylate (EHMA) and 2-(*N*,*N*-dimethylamino)ethyl methacrylate (DMAEMA) as monomer units of the MPC polymer, with the expectation of hydrophobic interactions and electrostatic attraction forces. The objective of this study was to modify the PDMS surface with the MPC polymer by simple treatment from aqueous solution, thereby negating the swelling effects of low-polarity solvents on PDMS. The influence of the electric charge of the polymer chain and the polymer conformation in aqueous solution on the modification of the PDMS surface is investigated herein by varying the ratio of water and ethanol in the mixture used as the solvent.

2. Experimental

2.1. Materials

MPC was synthesized according to a previously reported method [33]. EHMA, DMAEMA and sodium 1-anilino-8-naphtalene sulfonate (ANS-Na) were purchased from Tokyo Kasei Kogyo (Tokyo, Japan). Liquid PDMS (Silpot 184®) and its curing agent were purchased from Toray-Dow Corning Asia Co. The other reagents and solvents were commercially available in extra-pure grade and used without further purification.

2.2. Synthesis of positively charged amphiphilic polymer

Poly(MPC-*co*-EHMA-*co*-DMAEMA) (PMED) and poly(MPC-*co*-EHMA) (PMEH) were synthesized by a conventional radical polymerization method in ethanol using 2,2′-azobisisobutyronitrile (AIBN) as the radical initiator. The polymerization was carried out at 60 °C. The formed polymer was purified by pouring the reaction mixture into an excess volume of ether/chloroform (8/2, v/v) for precipitation. Furthermore, unreacted MPC was removed by crushing the precipitated polymer and washing with water for 2.0 h. The polymer was collected by filtration and lyophilized. The chemical structure of the polymer was confirmed by ^{1}H NMR in CD_3CD_2OD, the molecular weight of the polymer was evaluated by gel permeation chromatography (GPC, Jasco, Tokyo, Japan) using hexafluoroisopropanol (HFIP) as the eluent, and the retention time was compared with that of the poly(methyl methacrylate) standard. The chemical structure of PMED and PMEH is shown in Fig. 1.

2.3. Fluorescence measurement using ANS-Na

The polarity of the PMED and PMEH solutions prepared in a mixed solvent with various ratios of ethanol and water was evaluated by fluorescence measurements using ANS-Na as a probe. The polymers were first completely dissolved in ethanol, and water was then added in a prescribed ratio. Subsequently, ethanolic ANS solution was added to each sample and the mixture kept in a dark place. The final polymer concentration was 1.0 wt% and the ANS-Na concentration was 1.0×10^{-5} M. The internal polarity of the polymer aggregate was estimated using the maximum wavelength from the fluorescence of ANS-Na (λ_{ex} = 350 nm, measurement range = 420–650 nm).

2.4. Preparation of PDMS

The precursor of PDMS and curing agent were mixed in a 10:1 (v/v) ratio. The mixtures were evenly spread on a dish and were placed under vacuum to remove air bubbles. The curing reaction was performed at 60 °C for 4.0 h.

2.5. Treatment process

PMED and PMEH were dissolved in ethanol and water was added in a given ratio. Ethanolic polymer (PMED and PMEH) solutions containing water at ratios of 0, 20, 50, and 80 v/v% were prepared and are hereafter referred to as PMED-0, 20, 50, and 80 and PMEH-0, 20, 50, and 80, respectively. The final polymer concentration was adjusted to 1.0 wt%. All PDMS substrates were washed with ethanol prior to the treatment process. The plates were dipped 5 times for a few seconds into the PMED solution and then dried in air. This process was repeated twice and the plates were then completely dried under vacuum.

2.6. Surface characterization

The hydrophilicity of the PMED- and PMEH-treated PDMS surfaces was evaluated by measurement of the air and water contact angles using a static contact angle goniometer (CA-W; Kyowa Interface Science Co., Tokyo, Japan). Water contact angles (θ_{water}) were measured under dry conditions and the air contact angles (θ_{air}) were measured in water. The PDMS substrate was cut to fit dimensions of 10 mm × 40 mm × 1.0 mm and 10 mm × 20 mm × 0.70 mm for the respective air and water contact angle measurements.

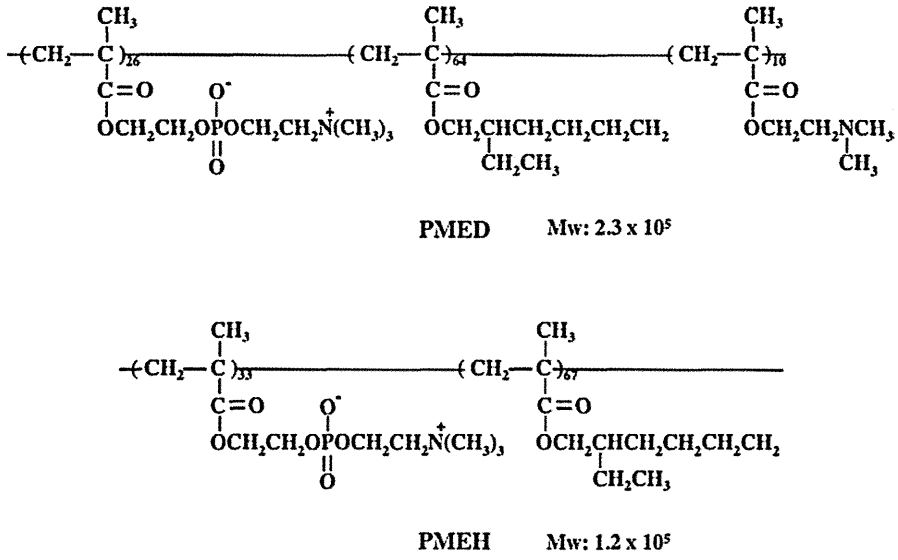

Fig. 1. Chemical structure of MPC polymers.

The polymer-treated samples were immersed in water for 1 h and were dried under vacuum before contact angle measurements. In the measurement of θ_{water} under dry conditions, water droplets were brought into contact with the modified PDMS surface and θ_{water} was measured within 10 s using photographic images. θ_{air} was measured in water by attaching the samples to a sample holder, which was then transferred into a glass holder filled with purified water. After 5 min, air bubbles were introduced underneath each sample through U-shaped needles and the contact angles were measured using photographic images. Data were collected at 10 positions for each sample. The stability of the polymer layer was evaluated by immersing the samples in water for 1.0, 24, 72, 120, and 168 h. The surface elemental composition was analyzed using X-ray photoelectron spectroscopy (XPS; AXIS-His165 Kratos/Shimadzu, Kyoto, Japan). The photoelectron take-off angle was fixed at 90°. All of the binding energies were referenced to the C_{1s} peak at 285.0 eV and the corresponding peak areas were used to calculate the respective elemental compositions.

2.7. Friction test

The coefficients of dynamic friction between a Co–Cr ball and the surface of the polymer-treated PDMS samples were measured using a surface property tester (Heidon Type32, Shinto Science Co., Tokyo, Japan). The PDMS substrates were prepared in the box (65 mm × 35 mm × 3.0 mm) and were affixed to the stage. The friction tests were performed in purified water at room temperature with load of 0.98 N, for a maximum of 1.0×10^3 cycles.

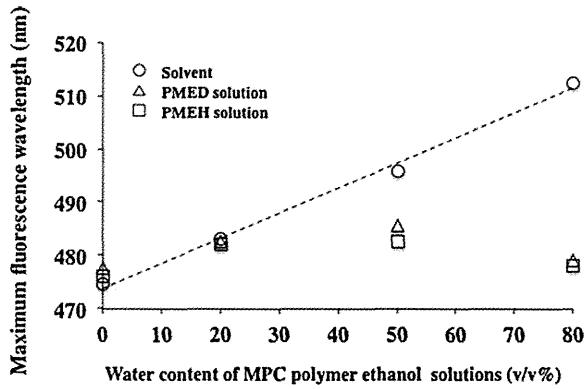

Fig. 2. Peak shifts of ANS-Na fluorescence in MPC polymer solutions.

The scan scale was 20 mm, and the scan speed was 40 mm/s. Three replicate measurements were performed for each sample, and the average values were regarded as the coefficients of dynamic friction.

3. Results and discussion

3.1. Characterization of the solubilized state of PMED in ethanol/water mixture

PMED and PMEH are both soluble in ethanol and do not dissolve in water. In addition, both polymers were soluble in ethanol/water mixtures. The polymer solution was transparent in water con-

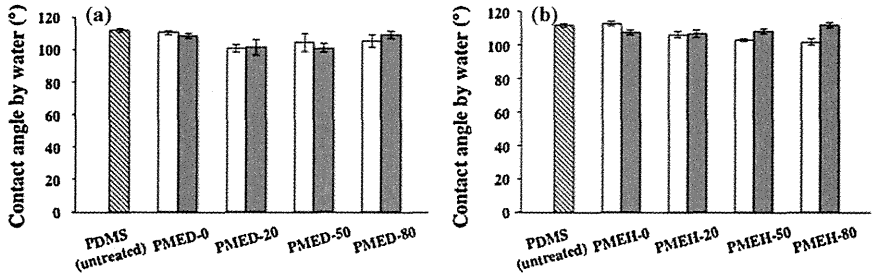

Fig. 3. The contact angles by water on the PDMS surface measured under dry conditions, before and after treatment with PMED (a) and PMEH (b) solution. Open column: just after treatment with the polymer solution. Closed column: after 1.0 h immersion in water.

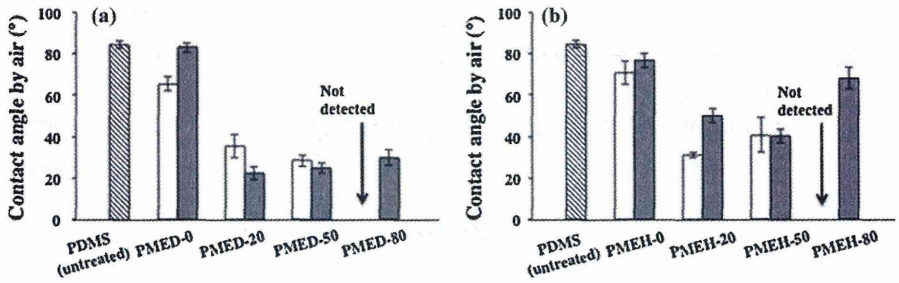

Fig. 4. The contact angles by air on the PDMS surface measured in aqueous solution, before and after coating with PMED (a) and PMEH (b) solution. Open column: just after coating. Closed column: after 1.0 h immersion in water.

tent ranges from 0 v/v% to 80 v/v%. Therefore, the conformation of the polymer changes in ethanol/water mixtures. The solubilized state of PMED and PMEH was evaluated after dissolution in ethanol/water mixtures of various ratios, using ANS-Na as a fluorescence probe. ANS-Na is sensitive to solvent polarity; the fluorescence quantum yield of ANS-Na is enhanced in hydrophobic environments, with a concomitant blue shift of the emission maximum [34]. Fig. 2 shows the emission maximum of ANS-Na in the solvent, PMED solution and PMEH solution. The maximum wavelength of fluorescence (λ_{max}) of ANS-Na in the 80 v/v% aqueous ethanolic solvent was 505 nm. However, the peak was blue-shifted with decreasing content of water. The λ_{max} of ANS-Na was almost the same in both the PMED and PMEH solutions. In the purely ethanolic and 20 v/v% aqueous-ethanolic polymer solutions, the λ_{max} of ANS-Na was almost same as that in the solvent. On the other hand, in the 50 v/v% and 80 v/v% aqueous-ethanolic polymer solutions, the λ_{max} was considerably lower than that in the solvent. The ratio of hydrophilic to hydrophobic units is almost same in both PMED and PMEH. These results indicate that both of the polymers undergo aggregation with increasing water content by hydrophobic interactions. In the 80 v/v% aqueous-ethanolic polymer solution, the polarity of the inside of the polymer aggregate was almost the same as that of ethanol.

3.2. Surface characterization of modified PDMS

The effect of the polymer conformation on the modification of the PDMS surface was investigated after dissolving PMED and PMEH in solvents with different ratios of ethanol to water. Fig. 3 shows the values of contact angles by water (θ_{water}) on the PDMS surface before and after treatment with PMED (a) and PMEH (b). In all samples, high values were obtained for the water contact angles under dry conditions, which were the same as those of untreated PDMS, and the values were not changed after immersion in water for 1 h. The phosphorylcholine group of the MPC polymers is hydrophilic, however, the hydrophobic units of the polymer are enriched at the air interface to decrease the surface free energy [35]. Fig. 4 shows the values of contact angles by air (θ_{air}) on the PDMS surface before and after treatment with PMED (a) and PMEH (b). In contrast to θ_{water} under dry conditions, θ_{air} in water were drastically decreased on the PMED and PMEH-treated surfaces, relative to the untreated surface, with the exception of the surface treated with PMED-0 and PMEH-0 (i.e., purely ethanolic) solutions. θ_{air} could not be measured on the surfaces treated with PMED-80 and PMEH-80, because the air bubble did not attach to the surface. The hydrophilic phosphorylcholine group is exposed in aqueous environments to reduce the interfacial free energy, thus, these results indicate successful treatment of the PDMS surface with PMED-20, 50, and 80 and PMEH-20, 50, and 80. After immersion in water for 1.0 h, the surfaces treated with PMED-20, 50, and 80 maintained their hydrophilicity. However, the contact angles of the surfaces treated with PMEH-20, 50, and 80 were increased after immersion in water for 1.0 h. In particular, the θ_{air} value of the surface treated with PMEH-80 was increased from 0° to 70°. These results indicate that PMEH-20, 50, and 80 were attached to the PDMS surface via weak interactions, and the polymer layer could be easily removed from the PDMS surface during immersion in aqueous solution. The success of the surface treatment with PMED and PMEH was further evaluated by XPS measurement. In the case of the surfaces treated with PMED-20, 50, and 80 and PMEH-20, 50, and 80, ammonium nitrogen and phosphorous peaks were observed at 403 eV and 133 eV, respectively. These atoms were attributed to the MPC unit. On the other hand, there were no peaks in the nitrogen region and phosphorous region for the surfaces treated with PMED-0 and PMEH-0. The results of the XPS and θ_{air} measurements reveal that when ethanol was used as a solvent (in the absence of water), the PDMS surface treatment process was unsuccessful. Fig. 5 shows the relationship between θ_{air} on the PDMS surfaces treated with PMED and PMEH versus the atomic ratio of P/Si of the surface. Contact angle and XPS values after immersion in water for 1.0 h were used for this plot. The atomic ratio of P/Si corresponded to the surface density of the MPC unit; therefore, the density of the phosphorylcholine group could be evaluated on this basis. The contact angle decreased

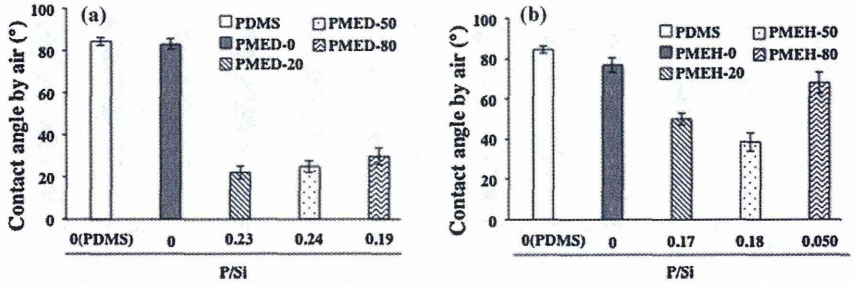

Fig. 5. Atomic ratio of P/Si on the PDMS surface coated with various MPC polymer solutions versus the air contact angles in an aqueous solution.

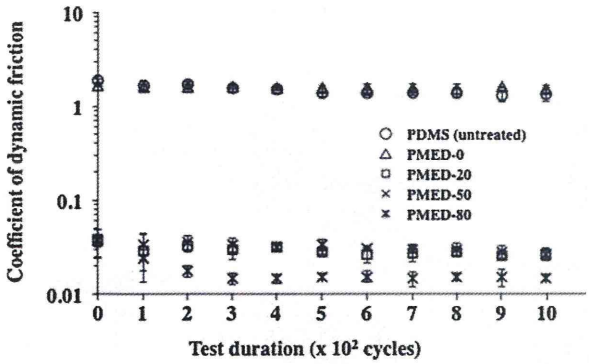

Fig. 6. Time course of the dynamic friction coefficient of the PDMS surface coated with PMED solution.

with an increase in the atomic ratio of P/Si, indicating that the wettability was conferred by the hydrophilic phosphorylcholine group.

3.3. Lubrication property

The lubricity of the surface is important for biomedical devices such as catheters, endoscopes, and artificial joints [19]. The dynamic friction coefficient was used as a parameter for characterizing the lubricity of the PDMS surface treated with PMED in water. Fig. 6 shows the time course of the dynamic friction coefficient between a Co–Cr ball and the surface of PMED-treated PDMS in water. The untreated PDMS surface and PMED-0 treated surface exhibited a very high dynamic friction coefficient of approximately 1.16, consistent with the unsuccessful treatment of the PDMS surface by PMED-0 indicated by the XPS and contact angle measurements. However, after treatment with PMED-20, 50, and 80, the dynamic friction coefficient was dramatically decreased to approximately 0.030, 0.030, and 0.015, respectively. This decrease is attributed to elimination of strong hydrophobic interactions by treatment with hydrophilic PMED. The hydrophilic state ensures the formation of an aqueous lubrication layer and reduces the friction force. The results of the lubrication tests corroborate with the results of the contact angle measurements. Furthermore, the low friction coefficient was maintained during 1.0×10^3 cycles at 0.98 N, demonstrating the stability of the PMED layer formed on the PDMS substrate during the treatment process.

3.4. Stability of MPC polymer on PDMS surface

The stability of the PMED and PMEH layers on the PDMS substrate in aqueous environments was further evaluated by XPS following surface treatment. Fig. 7 shows time course of the elemental ratio of P/Si for the PDMS surfaces treated with PMED (a) and PMEH (b). After immersion in water for 24 h, the atomic ratio of P/Si on the surface treated with PMED-50 and 80 decreased from 0.25 to 0.10. On the other hand, the atomic ratio of P/Si was maintained at 0.25 on the surface treated with PMED-20. All of the treated surfaces maintained an atomic ratio of P/Si of approximately 0.05 over the course of 168 h.

We have previously expounded the relationship between the amount of adsorbed fibrinogen and the surface P/Si ratio [36]. From that study, it is known that the fibrinogen adsorption capacity of the untreated PDMS surface is approximately 1.9 μg/cm^2. The amount of adsorbed fibrinogen was found to decrease with an increase in the atomic ratio of P/Si. In the case of a surface having an atomic ratio of P/Si of 0.035, the amount of fibrinogen adsorbed was significantly reduced to approximately 75% of that observed for the untreated PDMS. On this basis, it is predicted that the surface treated with PMED should exhibit good biofouling resistance after immersion in water for 168 h.

For the surfaces treated with PMEH-20 and 50, the atomic ratio of P/Si decreased from 0.25 to below 0.05 after immersion in water for 24 h, and for the surface treated with PMEH-80, the decrease was even more drastic, moving from approximately 0.15 to 0.05 over an immersion period of only 1.0 h. The P/Si ratio declined to almost 0 after immersion in water for 72 h for all of the treated surfaces. The pK_a of poly(DMAEMA) is about 8.0 [37,38]. In water (pH 5.6), more than 90% of the dimethyl amino groups are protonated. Therefore, PMED is positively charged and was more strongly adsorbed than PMEH; in particular, PMED-20 exhibited the highest stability among all the tested PMED types.

Fig. 8 shows an illustration of the relationship between the solubilized state of the polymer and the adsorption behavior of the polymer on the PDMS substrate. On the basis of the fluorescence measurements using ANS-Na, it was evident that neither PMED nor PMEH could form hydrophobic domains in the purely ethanolic and 20 v/v% aqueous-ethanolic solutions. On the other hand, hydrophobic domains were formed in the 50 v/v% and 80 v/v% aqueous-ethanolic solutions. In purely ethanolic solution, the hydrophobic interaction and electrostatic attraction forces were not operative between the polymer chains and the PDMS surface, therefore, there was no attachment of PMED and PMEH to the surface. In the 20 v/v% aqueous-ethanolic solutions of both polymers, the polymer chains were in the stretched conformation, and were adsorbed on the PDMS surface via hydrophobic interactions. However, the stability of the PMED layer on the surface was much higher than that of the PMEH layer. PMED possesses positive charges in the aqueous solution based on the DMAEMA units, whereas the PDMS surface is negatively charged. Therefore, the difference in the stability of the layers formed by PMED and PMEH suggests that PMED is adsorbed onto the PDMS surface not only by hydrophobic interactions but also by electrostatic attraction forces. In 50 v/v% and 80 v/v% aqueous-ethanolic solutions, PMED and PMEH could form aggregates, with hydrophobic interaction operating as the driving force for aggregation of the hydrophobic units. Because the hydrophobic domain was formed inside the polymer aggregate

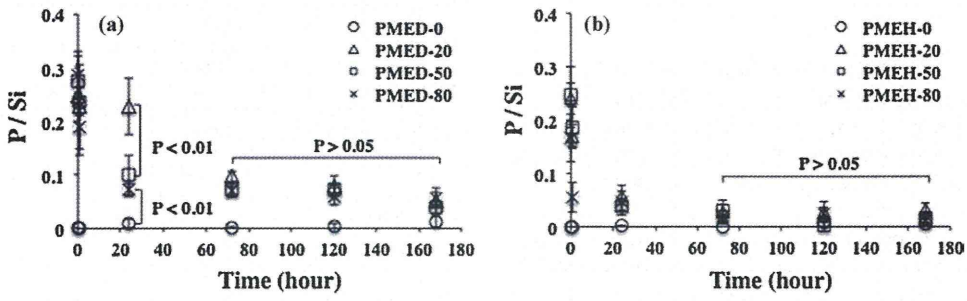

Fig. 7. Time course of the atomic ratio of P/Si on the PDMS surface coated with PMED (a) and PMEH (b) solution.

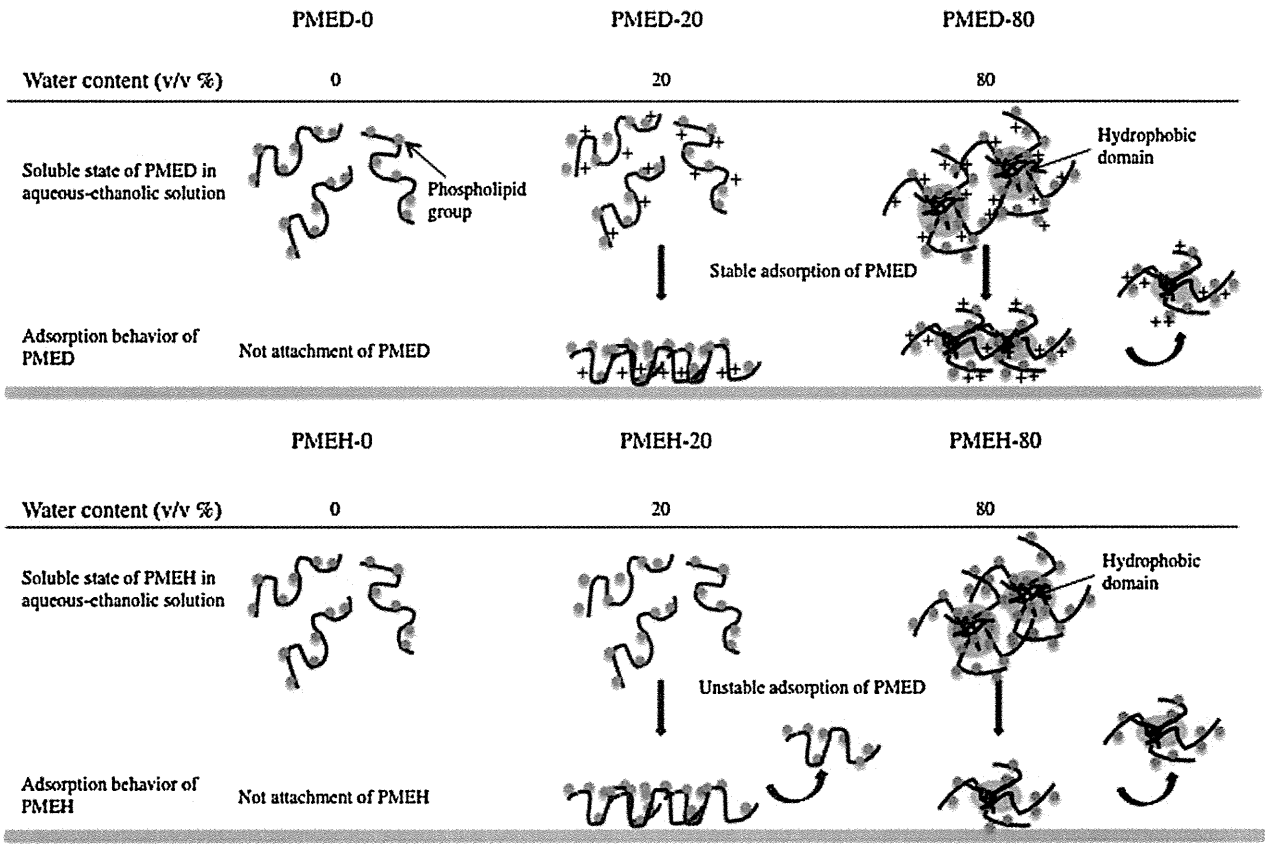

Fig. 8. Schematic illustration of the conformation of PMED and PMEH in aqueous-ethanolic solution and adsorption behavior of PMED and PMEH at PDMS surface.

and the hydrophobic interaction between the polymer chains and the PDMS surface was weakened, PMEH was weakly adsorbed on the PDMS surface. On the other hand, PMED was adsorbed on the PDMS surface primarily via electrostatic forces. Thus, PMED and PMEH may attach to the PDMS surface via either hydrophobic interaction or electrostatic attraction forces. However, both interactions are essential for stable binding between the polymer chains and the PDMS surface. The conformation of a protein is changed after adsorption; the hydrophobic inner surfaces are turned to the outside, and hydrophobic interaction between amino residues and the surface becomes stronger. This is due to the flexible and fragile conformation of proteins. The polymer aggregate is rigid and thermodynamically stable; therefore, the hydrophobic inner region cannot be turned to the outside after adsorption. Thus, the polymer must exist as discrete units in aqueous solution for formation of a stable surface layer, because the hydrophobic interaction between the polymer chains and the surface is weak in the aggregated state.

4. Conclusion

The surface properties of PDMS were readily modified by a simple treatment process using aqueous-ethanolic PMED and PMEH solutions without the need for any pretreatment process. After treatment, the PDMS surface exhibited good water wettability and the dynamic friction coefficient of the surface was decreased by nearly 80% compared with that of the untreated PDMS surface. We demonstrated that the positive charge and hydrophobic moiety were both needed in the polymer for the formation of a stable treatment during treatment of PDMS. Further, we found that the conformation of the polymer in solution influenced the adsorption process. This treatment process is simple and it is possible to apply to various devices made of PDMS after fabrication.

References

[1] M. Chhabra, J.M. Prausnitz, C.J. Radke, Biomaterials 28 (2007) 4331.
[2] M.K. Horne III, K.J. Brokaw, Thromb. Res. 112 (2003) 111.
[3] T.J. Joyce, A. Unsworth, Wear 250 (2001) 199.
[4] J.G. Alauzum, S. Young, R. D'Souza, L. Liu, M.A. Book, H.D. Sheardown, Biomaterials 31 (2010) 3471.
[5] A. Wu, B. Zhao, Z. Dai, J. Qin, B. Lin, Lab Chip 6 (2006) 942.
[6] Y. Yuan, X. Zang, F. Ai, J. Zhou, J. Shen, S. Lin, Polym. Int. 53 (2004) 121.
[7] S. Pintro, P. Alves, C.M. Matos, A.C. Santos, L.R. Rodrigues, J.A. Teixeira, M.H. Gil, Colloids Surf. B: Biointerfaces 81 (2010) 20.
[8] H. Makamba, Y.Y. Hsieh, W.C. Sung, S.H. Chen, Anal. Chem. 77 (2005) 3971.
[9] M. Farrell, S. Beaudoin, Colloids Surf. B: Biointerfaces 81 (2010) 468.
[10] H. Chen, Z. Zhang, Y. Chen, M.A. Brook, H.D. Sheardown, Biomaterials 26 (2005) 2391.
[11] M. Ouyang, C. Yuan, R.J. Muisener, A. Boulares, J.T. Koberstein, Chem. Mater. 12 (2000) 1591.
[12] D. Bodas, C.K. Malek, Microelectr. Eng. 83 (2006) 1277.
[13] M. Morra, E. Occhiello, R. Marola, F. Garbassi, P. Humphrey, D. Johnson, J. Colloid Interface Sci. 137 (1990) 11.
[14] Y. Inoue, T. Nakanishi, K. Ishihara, React. Funct. Polym. 71 (2011) 350.
[15] R. Matsuno, K. Ishihara, NanoToday 6 (2011) 61.
[16] K. Ishihara, N.P. Ziats, B.P. Tierney, N. Nakabayashi, J.M. Anderson, J. Biomed. Mater. Res. 25 (1991) 1397.
[17] K. Ishihara, H. Nomura, T. Mihara, K. Kurita, Y. Iwasaki, N. Nakabayashi, J. Biomed. Mater. Res. 39 (1998) 323.
[18] M. Kyomoto, Y. Iwasaki, T. Moro, T. Konno, F. Miyaji, H. Kawaguchi, Y. Takatori, K. Nakamura, K. Ishihara, Biomaterials 28 (2008) 3121.
[19] M. Kyomoto, T. Moro, K. Saiga, F. Miyaji, H. Kawaguchi, Y. Takatori, K. Nakamura, K. Ishihara, Biomaterials 31 (2010) 658.
[20] S.H. Ye, C.A. Johnson Jr., J.R. Woolley, H. Murata, L.J. Gamble, K. Ishihara, W.R. Wagner, Colloids Surf. B: Biointerfaces 79 (2010) 357.
[21] T. Simizu, T. Goda, N. Minoura, M. Takai, K. Ishihara, Biomaterials 31 (2010) 3274.
[22] T. Moro, Y. Takatori, K. Ishihara, T. Konno, Y. Takigawa, T. Matsushita, U.I. Chung, K. Nakamura, H. Kawaguchi, Nat. Mater. 3 (2004) 829.
[23] T. Moro, H. Kawaguchi, K. Ishihara, M. Kyomoto, T. Karita, H. Ito, K. Nakamura, Y. Takatori, Biomaterials 30 (2009) 2995.

[24] T. Goda, T. Konno, M. Takai, T. Moro, K. Ishihara, Biomaterials 27 (2006) 5151.
[25] T. Goda, R. Matsuno, T. Konno, M. Takai, K. Ishihara, Colloids Surf. B: Biointerfaces 63 (2008) 64.
[26] Y. Iwasaki, M. Takamiya, R. Iwata, S. Yusa, K. Akiyoshi, Colloids Surf. B: Biointerfaces 57 (2007) 226.
[27] J. Sibarani, M. Takai, K. Ishihara, Colloids Surf. B: Biointerfaces 54 (2007) 88.
[28] J.H. Seo, R. Matsuno, T. Konno, M. Takai, K. Ishihara, Biomaterials 29 (2008) 1367.
[29] A. Lee, N.D. Spencer, Tribol. Int. 38 (2005) 922.
[30] S. Lee, R. Iten, M. Muller, N.D. Spencer, Macromolecules 37 (2004) 8349.
[31] S. Lee, N.D. Spencer, Langmuir 24 (2008) 9479.
[32] M. Rabe, D. Verdes, S. Seeger, Adv. Colloid Interface Sci. 162 (2011) 87.
[33] K. Ishihara, T. Ueda, N. Nakabayashi, Polym. J. 22 (1990) 355.
[34] T. Konno, J. Watanabe, K. Ishihara, Biomacromolecules 5 (2004) 342.
[35] K. Futamura, R. Matsuno, T. Konno, M. Takai, K. Ishihara, Langmuir 24 (2008) 10340.
[36] K. Ishihara, B. Ando, M. Takai, Nanobiotechnology 3 (2007) 83.
[37] M.J. Bruining, H.G.T. Blaauwgeers, R. Kuijer, E. Pels, R.M.M.A. Nuijts, L.H. Koole, Biomaterials 21 (2000) 595.
[38] A.M. Funhoff, C.F.V. Nostrum, G.A. Koning, N.M.E.S. Nieuwenbroek, D.J.A. Crommelin, W.E. Hennink, Biomacromolecules 5 (2004) 32.

Acta Biomaterialia 8 (2012) 860–865

Contents lists available at SciVerse ScienceDirect

Acta Biomaterialia

journal homepage: www.elsevier.com/locate/actabiomat

Electrically polarized micro-arc oxidized TiO_2 coatings with enhanced surface hydrophilicity

Chufan Ma [a,b], Akiko Nagai [a,*], Yuko Yamazaki [a,c], Takeshi Toyama [c], Yusuke Tsutsumi [d], Takao Hanawa [d], Wei Wang [a], Kimihiro Yamashita [a]

[a] Department of Inorganic Materials, Institute of Biomaterials and Bioengineering, Tokyo Medical and Dental University, 2-3-10 Kanda-Surugadai, Chiyoda-ku, Tokyo 101-0062, Japan
[b] Department of Prosthodontics, School of Stomatology, Fourth Military Medical University, 145, Changlexi Road, Xi'an 710032, People's Republic of China
[c] Department of Materials and Applied Chemistry, College of Science and Technology, Nihon University, 1-8-14 Kanda-Surugadai, Chiyoda-ku, Tokyo 101-8308, Japan
[d] Department of Metals, Institute of Biomaterials and Bioengineering, Tokyo Medical and Dental University, 2-3-10 Kanda-Surugadai, Chiyoda-ku, Tokyo 101-0062, Japan

ARTICLE INFO

Article history:
Received 29 March 2011
Received in revised form 9 August 2011
Accepted 20 September 2011
Available online 24 September 2011

Keywords:
TiO_2 coatings
Micro-arc oxidation
Electric polarization
Hydrophylicity
Oxygen vacancy

ABSTRACT

The use of micro-arc oxidation titania (MAO TiO_2) coatings to modify titanium surfaces improves the biocompatibility of implant surfaces. To obtain hydrophilic MAO TiO_2 coating surfaces electric polarization, which induces surface electric fields in the materials and produces surface charges, was performed in this study. Electric polarization of the MAO TiO_2 coatings was confirmed by measuring the thermally stimulated depolarization current. After electric polarization treatment the MAO TiO_2 coatings did not exhibit any obvious changes in surface roughness, morphology, or phase components. X-ray photoelectron spectroscopy results indicated that electric polarization resulted in oxidation of the cathodic-faced surfaces and reduction of the anodic-faced surfaces. This result suggests that the existence of a concentration gradient of oxide ions/oxygen vacancies produced the stored space charge in the coatings. Reduction of the deionized water contact angle on the polarized MAO TiO_2 surfaces was maintained for longer periods compared with the non-polarized surface. Our study demonstrated that metastable electric fields across the MAO TiO_2 coating produced by electric polarization made it durably wettable by reducing the interfacial surface tension between the material and water.

1. Introduction

Titanium is one of the most widely used biomaterials for dental and orthopedic implants [1,2]. The surface oxide layer is considered an important factor in favorable interactions between tissues and implants [3]. A number of physical and chemical TiO_2 coating methods have been proposed to improve the biocompatibility of implant surfaces [4]. Among them, micro-arc oxidation (MAO), an electrochemical procedure for modifying Ti surfaces, has attracted a great deal of attention [5–7]. The MAO TiO_2 coating is both porous and firmly adheres to the substrate, and both properties are beneficial to the biological performance of the implants. Another advantage of this MAO process is the possibility of incorporating Ca and P ions into the surface coating, by controlling the composition and concentration of the electrolyte, as previous studies have shown that Ca and P phases are beneficial to the bioactivity of the specimens [8,9]. Bioactivity is the ability to communicate with the living body directly. Moreover, this process is well suited to modifying a number of metal substrates with complex geometries, producing an effective chemical barrier against the release of metal ions from the substrate, and can enhance the corrosion resistance of titanium alloys. In the last decade many studies on the biological response to titanium implants have demonstrated that the MAO process constitutes one of the most effective methods of modifying the implant surface [10–12].

Our previous studies showed that electric polarization can be utilized to induce surface electric fields under a d.c. field in bioceramics such as hydroxyapatite (HAp), β-tricalcium phosphate, carbonated hydroxyapatite and bioglasses [13–16]. Surface electric fields in polarized HAp have been experimentally demonstrated in vitro to affect the interfaces between charged surfaces and ions, proteins and cultured cells [17–20]. In vivo surface electric fields also have a remarkable ability to enhance new bone formation on various polarized HAp geometries [21,22]. Moreover, the surface wettability of HAp can be improved by a inducing surface charge via polarization [19,20].

Wettability is an important property of biomaterials because cell adhesion, spreading and differentiation are generally better on hydrophilic surfaces [23,24]. Untreated MAO TiO_2 is known to have a hydrophobic surface. Many studies have reported that MAO TiO_2 surfaces can be made hydrophilic in ambient air by thermal

* Corresponding author. Tel.: +81 352808017; fax: +81 352808015.
E-mail address: nag-bcr@tmd.ac.jp (A. Nagai).

1742-7061/$ - see front matter © 2011 Acta Materialia Inc. Published by Elsevier Ltd. All rights reserved.
doi:10.1016/j.actbio.2011.09.021

annealing, chemical treatment, or UV illumination [8,25,26], however, the hydrophilic MAO TiO_2 becomes hydrophobic over time.

This study investigates the possibility of using electric polarization to make MAO TiO_2 coatings durably wettable. The effects of electric polarization on the microstructure and surface characteristics of the coating were also analyzed.

2. Materials and methods

Titanium discs (ϕ 10 × 2 mm) were fabricated with commercially pure titanium (grade 2) and were successively ground using grade 320 and 600 waterproof abrasive paper to remove the natural surface oxide. The samples were then ultrasonically cleaned in acetone, ethanol and distilled water. The titanium discs were subjected to a modified MAO treatment according to previous studies [8,27]. Anodizing was performed in an aqueous electrolyte at 400 V for 5 min by applying a d.c. field to the samples. The electrolyte contained 0.15 M calcium acetate monohydrate ($(CH_3COO)_2$-$Ca{\cdot}H_2O$, Wako, Japan) and 0.02 M calcium glycerophosphate ($C_3H_7CaO_6P$, Wako, Japan). All of the MAO processing was carried out in a water-cooled bath, with a stainless steel plate was used as the cathode. A magnetic stirrer was used to achieve homogeneity in the electrolyte and to eliminate air bubbles generated on the titanium surface during the process. After MAO treatment the samples were rinsed with distilled water and dried in an oven at 40 °C for 24 h. The samples were uniformly light gray.

In accordance with the electric polarization process reported in previous works [13–15] the MAO TiO_2 coated samples were sandwiched between a pair of platinum (Pt) plate electrodes, electrically polarized in a d.c. field of 5 kV cm^{-1} in air at 400 °C for 1 h and then cooled to room temperature under the applied d.c. voltage. The TiO_2 coating in contact with the anode was termed the negative surface (N surface), and the TiO_2 coating placed in contact with the cathode was called the positive surface (P surface). A non-polarized specimen was heated in air at 400 °C for 1 h under no field and termed the 0 surface.

The thermally stimulated depolarization current (TSDC) of the polarized samples were measured with a Hewlett–Packard 4140B pA meter. Each polarized sample was sandwiched between Pt electrodes and heated to 550 °C in an electric furnace equipped with a stainless steel shielded sample chamber at a heating rate of 5 °C min^{-1}. The total amount of stored charge was calculated as previously reported [17].

The surface morphologies and cross-sectional microstructures of the coatings before and after polarization were observed by scanning electron microscopy (SEM) (Hitachi S-3400NX, Tokyo, Japan). In addition, the elemental compositions and distributions of the coatings were also analyzed using energy-dispersive X-ray spectroscopy (EDX) in conjunction with the SEM system.

The phase compositions of the sample surfaces were analyzed by X-ray diffraction (XRD) (PW1700, PANalytical, Tokyo, Japan) in the 2θ range 10–70° using CuK_α radiation at 40 kV and 10 mA.

The chemical compositions of the sample surfaces were analyzed by X-ray photoelectron spectroscopy (XPS) (SSX-100, Surface Science Instruments, Mountain View, CA, USA) under ultrahigh vacuum. MgK_α (1253.6 eV) radiation was used as the X-ray source in the XPS tests. The XPS take-off angle was set to 90°. Charge effects were corrected using the C1s line of adventitious carbon at 285 eV. The XPS spectra were fitted using the Casa program to a Gaussian–Lorentzian peak shape with a Shirley baseline to represent the background. The composition of the coatings and thickness of the contaminant carbon layer were calculated according to methods used in a previous study [28].

The surface roughnesses of the samples were quantified using a laser profile micrometer (VF-7500, Keyence, Osaka, Japan) with a resolution of 0.01 μm. Six samples from each group were chosen at random and scanned. The scans were performed at three different positions on each sample. The R_a values are presented as means ± SD.

Contact angle measurements were performed using the sessile drop method at room temperature with a commercial contact angle meter (Kyowa Interface Measurement and Analysis System, Tokyo, Japan). Images were collected with a camera and the contact angle between the 1 μl droplet of deionized water and the coated surface was measured from the magnified image. Five samples from each group were used for contact angle measurement. The measurements were performed three times at different positions on each sample.

All values are presented as means ± SD, and commercial statistical software (Statcel, OMS Ltd, Saitama, Japan) was used for statistical analysis. One-way analysis of variance (ANOVA) was used following multiple comparisons with Scheffe's *F*-test to assess the data, and $P < 0.05$ was considered to indicate statistical significance.

3. Results and discussion

3.1. Structure and morphology of the MAO TiO_2 coatings

The surface morphology, cross-sectional microstructure, elemental compositions and distributions of the MAO TiO_2 coating are shown in Figs. 1 and 2. The figures show that a porous layer was formed on the surface of the Ti substrate after MAO treatment, with pore sizes of about 2–4 μm distributed homogeneously (Fig. 1a). These pits were optimized to produce an implant surface for interaction with bone [29]. The cross-section image reveals that the coating was approximately 10 μm thick (Fig. 1b). The EDX spectra demonstrate the presence of C, O, Ca, P and Ti (Fig. 2a). The Ca and P elements were incorporated and distributed homogeneously through the coating after MAO treatment (Fig. 2b). The Ca:P atomic ratio was 1.5.

The XRD patterns of the polarized and non-polarized MAO TiO_2 coatings are shown in Fig. 3. The MAO TiO_2 coating consisted of 32% rutile and 68% anatase. The phase content of TiO_2 was obtained using the Spurr equation [30]:

$$W_R = 1 - 1/(1 + 1.26(A_R/A_A)) \quad (1)$$

where W_R is the rutile content and A_A and A_R represent the diffraction intensities of anatase (101) and the rutile (110), respectively. The ratio between the rutile and anatase contents was controlled by the applied voltage [31]. Despite the existence of Ca and P in the electrolyte no Ca- or P-containing phases were detected by XRD [6]. The average MAO TiO_2 crystal size calculated from the (101) peak of anatase and the (110) peak of rutile was the same as that of pure TiO_2. There were no obvious changes in morphology or phase composition after electric polarization.

3.2. Spectroscopic investigation of the surface

XPS surveys of the MAO TIO_2 coatings were performed before and after electric polarization (Fig. 4a). The elements with the highest detected concentrations were Ti, O, C, Ca and P (Table 1). The atomic concentration (%) of each element in MAO TIO_2 was stable under polarization. The amount of organic contaminants, thickness 5 Å, in the surfaces also remained constant after polarization.

High resolution XPS spectra of O1s, Ca2p, P2p and Ti$2p_{3/2}$ were measured from the MAO coatings before and after electric polarization. The Ca2p spectra of the MAO surfaces reveal that the surface exhibits the typical double peak feature at 347.5 eV ($2p_{3/2}$) and 351.0 eV ($2p_{1/2}$) with a spin orbit splitting of 3.5 eV. This observation

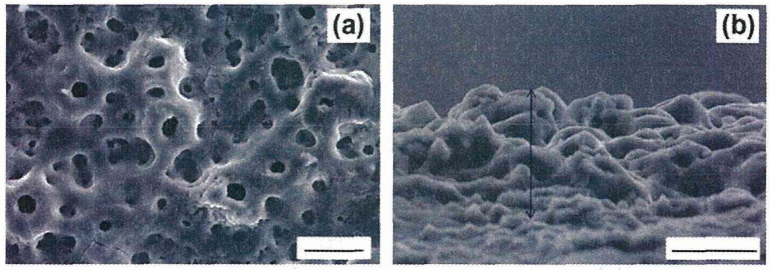

Fig. 1. SEM images of (a) a top view and (b) an oblique view (40°) of MAO TiO_2. An arrow indicates the coating range. The bar represents 10 μm.

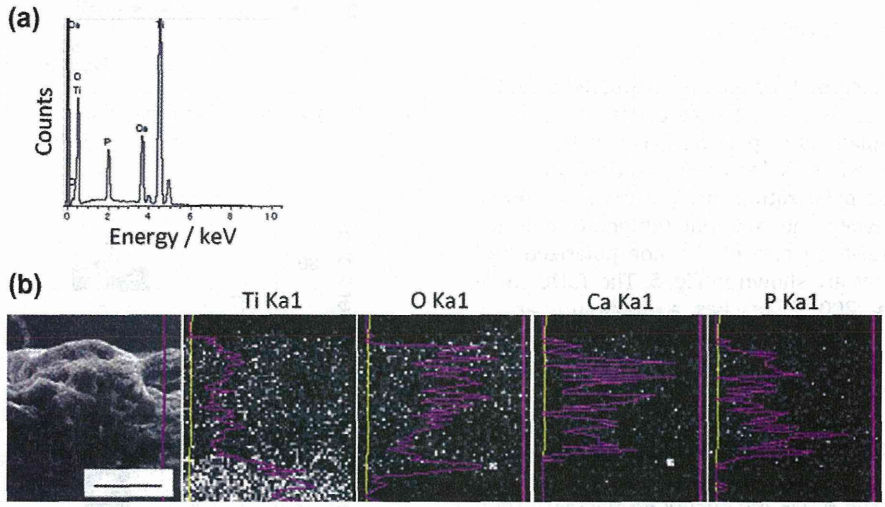

Fig. 2. EDX spectra of (a) a surface scan, (b) a line scan of a cross-section of the MAO TiO_2 coating. The bar represents 10 μm.

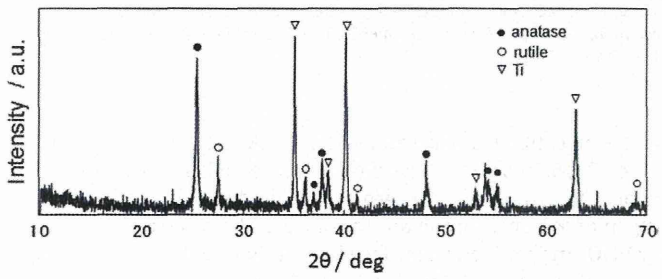

Fig. 3. XRD spectra of the MAO TiO_2 coating.

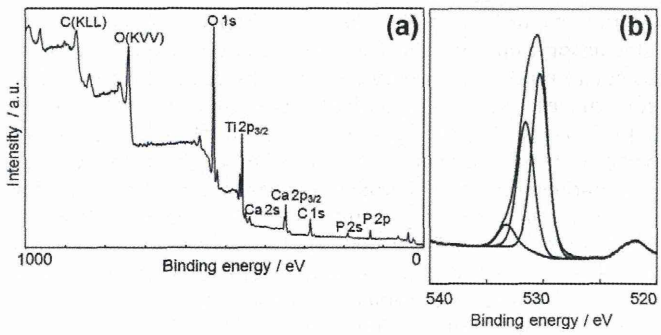

Fig. 4. Surveys of (a) the XPS spectra and (b) the O1s high resolution spectra of the non-polarized MAO TiO_2 coating.

provides evidence for divalent Ca-containing surface species [27]. The P2p spectra exhibited a single peak at 133.5 eV, suggesting that phosphorus exists in the samples in the pentavalent oxidation state

Table 1
Elemental composition detected by XPS.

Sample	Elemental composition (at.%)			
	O	Ti	Ca	P
0 surface	73	14	7	6
P surface	73	15	7	5
N surface	73	15	7	5

(P^{5+}) [27]. Ti–P bonds were not observed in the samples because the characteristic peak of P in Ti–P at 129 eV was not present in the spectra. No discernible changes were observed in the peak positions or full widths at half maximum (FWHM) of the Ca2p and P2p spectra after polarization. The $Ti2p_{3/2}$ spectrum was resolved into three spin orbit components according to the oxidation states at binding energies (BE) of 455.2, 457.0 and 459.1 eV, which represent the TiO, Ti_2O_3 and TiO_2 fractions in the samples, respectively [32]. The intensities of the deconvoluted components show that the dominant surface state is Ti^{4+} on all surfaces, and the intensity ratios of Ti^{4+} of the samples are all the same. This result indicates that polarization has little effect on the Ti state of MAO TiO_2 coatings. The O1s spectra were deconvoluted into three kinds of oxygen bonds at BE of 530.5, 531.7 and 533.5 eV, which represent oxide species (O^{2-}), dissociative water (hydroxyl groups)/phosphate groups (OH^- or PO_4^{3-}) and adsorped molecular water (H_2O), respectively (Fig. 4b) [33,34]. The area ratios of the three peaks in the O1s spectra of the different surfaces are listed in Table 2. The intensities of the H_2O spectra from the polarized specimens were enhanced compared with those of the non-polarized samples. The largest surface OH groups/O^{2-} ratio of 54% was found at the P surface, followed by 53% at the 0 surface and 44% at the N surface. This result suggests that the P surface

Table 2
Percentage areas of the deconvoluted peaks in the O1s XPS spectra.

Sample	Percentage area		
	530.5 eV	531.7 eV	533.5 eV
0 surface	60	32	7.4
P surface	59	32	8.0
N surface	63	28	8.1

was the most reduced of all of the specimens, while the N surface retained an oxidizing state. There were oxygen and oxygen vacancy distribution gradients in the three samples.

3.3. TSDC spectrum and stored electric charge

The behavior of a polarized material can be estimated by TSDC measurements. TSDC analysis is a widely used experimental technique to investigate the qualities of polarized materials such as stored charges, activation energies for depolarization processes and relaxation times. Ionic polarization inside a material causes the generation of TSDC when the material temperature is increased. Representative TSDC spectra of the non-polarized and polarized MAO TiO_2 samples are shown in Fig. 5. The TSDC curve begins to increase at ca. 200 °C, reaches a maximum at ca. 500 °C, and then gradually decreases. The average stored charges of the non-polarized specimen and the polarized samples calculated from the TSDC curves were 2.6 and 21 μC cm^{-2}, respectively. This result confirms that MAO TiO_2 coatings can be polarized under the experimental conditions utilized. These results also confirm that the polarized specimens maintain the same surface polarization state after 3 months. The activation energy for depolarization of MAO TiO_2 was 0.85 eV, calculated from the TSDC spectrum. The activation energy observed was close to the values of activation energy for conductivity reported for nanoporous TiO_2 films [35]. The result suggests that the charge carriers in electrical conduction of nanoporous TiO_2 films also play a role in the polarization of MAO TiO_2. The process underlying the polarization treatment can be explained as follows. Ti^{2+} and Ti^{3+} exist in MAO TiO_2, as shown in the XPS analysis, and oxygen vacancies (Vö) are present in the coating. Vö accumulate on the cathodic side (P surfaces) but are depleted on the anodic side (N surfaces) under a d.c. field and at elevated temperatures because Vö occur in TiO_2 ceramics [36]. Thus a Vö concentration gradient is produced. Oxygen and Vö should play essential roles in the electric polarization of TiO_2 under a d.c. field.

The samples enter a metastable state when they are cooled to room temperature and the d.c. field is removed. On the other hand, when the temperature is elevated in air, a slight reduction of the TiO_2 surface occurs, described by the reaction:

$$2O_O^{\times} \leftrightarrow 2V\ddot{o} + 4e' + O_2(g) \quad (2)$$

The electrons produced by this reaction cause currents in non-polarized TiO_2. That is to say, there are at least two polarization pathways responsible for the TSDC of the polarization samples. The currents responsible for space charge polarization remain after subtraction of the reduction currents.

3.4. Water contact angle on the surface

Fig. 6 shows the results of static water contact angle measurements on the MAO TiO_2 surfaces after heating only or after electric polarization. The initial water contact angle on the untreated surface was 73.1 ± 4.2°, which decreased to below 10° after heating or polarization. Four days later the water contact angle of the non-polarized surface returned to 62.5 ± 9.7°, but was 27.4 ± 11.4° on the P surface and 10.3 ± 2.1° on the N surface. One month later

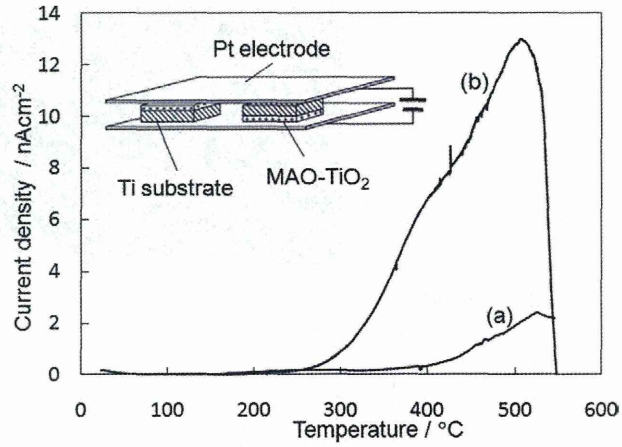

Fig. 5. Thermally stimulated depolarization current (TSDC) spectra of (a) non-polarized and (b) polarized MAO TiO_2 coatings and schematics of the polarization system.

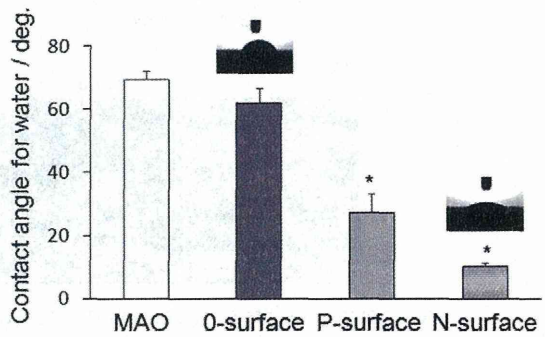

Fig. 6. Water contact angle measurements of the MAO TiO_2 coating and the 0 surface, N surface and P surface 4 days after heat or polarization treatment. Side view images of 1 μl of water dropped onto the 0 surface and N surface are also presented.

the water contact angle returned to 41.8 ± 3.1° on the P surface and 48.7 ± 5.5° on the N surface. Surface reduction mediated by the heat treatment may return over time due to the adsorption of oxygen or water from the air. In contrast, the electrically polarized MAO TiO_2 maintained its surface hydrophilicity. The surface roughnesses (R_a values) of the 0 surface, N surface and P surface are 1.2 ± 0.042, 1.2 ± 0.015 and 1.2 ± 0.035 μm, respectively, suggesting that polarization does not alter the surface roughness.

The MAO TiO_2 surface is subject to oxygen loss under thermal reduction conditions, and accordingly surface Vö are created. Water adsorption onto the TiO_2 surface is described by either a molecular or a dissociative mechanism. Dissociative water at oxygen vacancies results in two bridging OH groups for each vacancy site [37]. One of these OH groups can be thought of as comprising oxygen from the water molecule adsorbed at the vacancy, while the second results from hydrogen transfer to a neighboring bridging oxygen anion site. In principle these two bridging OH groups are indistinguishable. These surface OH groups result in superhydrophilicity at the surfaces immediately after heat treatment. The H_2O–TiO_2 interactions observed on thermal activation at oxygen vacancy sites are similar to interactions under UV illumination in that Ti^{3+} sites were formed [38,39]. However, it has been reported that reversible oxidation occurs in crystalline TiO_2 samples with thermal defects heated to high temperatures in air, and that the oxygen defects are rapidly compensated for [32]. This process causes the hydrophilicity of the 0 surface to change within several days. This result also suggests that high temperature treatment